Journal Pre-proof

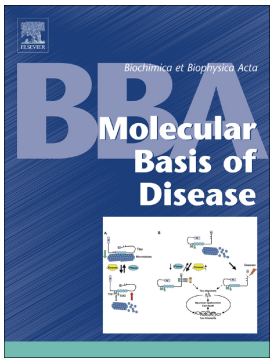

PGC1-α-driven mitochondrial biogenesis contributes to a cancer stem cell phenotype in melanoma

Fabrizio Fontana, Chiara Macchi, Martina Anselmi, Alessandra Stefania Rizzuto, Massimiliano Ruscica, Patrizia Limonta

PII: S0925-4439(23)00263-6

DOI: https://doi.org/10.1016/j.bbadis.2023.166897

Reference: BBADIS 166897

To appear in: *BBA - Molecular Basis of Disease*

Received date: 8 February 2023

Revised date: 1 September 2023

Accepted date: 21 September 2023

Please cite this article as: F. Fontana, C. Macchi, M. Anselmi, et al., PGC1-α-driven mitochondrial biogenesis contributes to a cancer stem cell phenotype in melanoma, *BBA - Molecular Basis of Disease* (2023), https://doi.org/10.1016/j.bbadis.2023.166897

PGC1-α-DRIVEN MITOCHONDRIAL BIOGENESIS CONTRIBUTES TO A CANCER STEM CELL PHENOTYPE IN MELANOMA

Fabrizio Fontana[1#], Chiara Macchi[1], Martina Anselmi[1], Alessandra Stefania Rizzuto[2], Massimiliano Ruscica[1,3], Patrizia Limonta[1]

[1]*Department of Pharmacological and Biomolecular Sciences "Rodolfo Paoletti", Università degli Studi di Milano, Milan, Italy.*

[2]*Department of Clinical Sciences and Community Health, Università degli Studi di Milano, Milan, Italy.*

[3]*Department of Cardio-Thoracic-Vascular Diseases, Foundation IRCCS Cà Granda Ospedale Maggiore Policlinico, Milan, Italy.*

[#]Corresponding author. Department of Pharmacological and Biomolecular Sciences "Rodolfo Paoletti", Università degli Studi di Milano, Via Balzaretti 9, 20133 Milan, Italy.

E-mail address: fabrizio.fontana@unimi.it

Phone number: +39 0250318427

ABSTRACT

Little is known about the metabolic regulation of cancer stem cells (CSCs) in melanoma. Here, we used A375 and WM115 cell lines to dissect the role of mitochondria in conferring CSC traits. Notably, we observed that A375 and WM115 melanospheres, known to be enriched in ABCG2+ CSCs, showed higher mitochondrial mass compared with their adherent counterpart. In particular, they displayed increased PGC1-α expression and oxidative phosphorylation (OXPHOS) complex levels, leading to a metabolic switch characterized by enhanced mitochondrial membrane potential, oxygen consumption, ATP synthesis and ROS production. Interestingly, PGC1-α silencing resulted in the suppression of CSC features, including clonogenic ability, migration, spheroid formation and ABCG2 enrichment. Similarly, XCT790 and SR-18292, two PGC1-α inhibitors, were able not only to reduce melanoma tumorigenicity and invasion but also to block melanosphere growth and propagation and ABCG2+ cell proliferation. In conclusion, improved mitochondrial biogenesis is associated with a stem-like phenotype in melanoma, and therapeutically targeting the mitochondria-enriched CSC subpopulation might overcome tumor progression.

Keywords: melanoma; cancer stem cells (CSCs); mitochondrial biogenesis; PGC1-α; oxidative phosphorylation (OXPHOS)

INTRODUCTION

Cutaneous melanoma is a very heterogeneous tumor [1,2]. This high heterogeneity has been widely associated with the existence of cancer stem cells (CSCs), a small self-renewing subpopulation able to give rise to the entire tumor mass via symmetric and asymmetric division. In this setting, CSCs represent the main drivers not only of cancer growth and metastasis but also of cancer chemoresistance and recurrence [1–3].

Recent studies have suggested that impairing oxidative phosphorylation (OXPHOS) in cancer cell mitochondria may represent a useful approach to suppress tumor growth and progression [4–6]. In particular, CSCs collected from various malignant tissues have been shown to display an oxygen-dependent metabolic profile characterized by a PGC1-α-mediated increase in mitochondrial mass, which has been recently proposed as a new biomarker for CSC identification and as a novel pharmacological target for cancer eradication [7–13]. However, little is known about this topic in melanoma.

Herein, we hypothesized that high mitochondrial content could specifically identify a melanoma SC subpopulation and could be exploited for the treatment of this tumor. Indeed, although we have recently demonstrated a close relationship between ATP-binding cassette transporter G2 (ABCG2) overexpression and melanoma stemness, a specific CSC-associated metabolic signature has not been found yet [14]. In this context, the present study aims at further characterizing melanoma SC traits, with a focus on the role of mitochondrial biogenesis in determining the emergence of a CSC phenotype.

MATERIALS AND METHODS

Chemicals

ABCG2 antibody (NB110-93511AF405) for flow cytometry was from Biotechne, Minneapolis, MN, USA.

The following primary antibodies were utilized for Western blot analysis: Total OXPHOS (ab110413) and PGC1-α (ab110411) from Abcam, Cambridge, UK; GAPDH (5174) from Cell Signaling Technology Inc., Danvers, MA, USA. All the antibodies were used at the concentration 1:1000, except for PGC1-α (utilized at 1:500). Horseradish-peroxidase-conjugated secondary antibodies and enhanced chemiluminescence reagents were from Cyanagen, Bologna, Italy.

Control siRNA (scramble, AM4611) and PGC1-α SiRNA (siPGC1-α, AM16704) were from Invitrogen Life Technologies, Monza, Italy. SR-18292 and XCT790 were purchased from Sigma-Aldrich, Milano, Italy.

Cell lines

A375 and WM115 human melanoma cell lines were purchased from American Type Culture Collection (ATCC, Manassas, VA, USA) and were cultured in DMEM medium supplemented with 7.5% FBS, glutamine and antibiotics, in humidified atmosphere of 5% CO2/95% air at 37°C. Original cell stocks were stored frozen in liquid nitrogen. After resuscitation, cells were kept in culture for no more than 10-12 weeks; they were detached through trypsin-EDTA solution and passaged once/week.

To obtain melanospheres, A375 and WM115 cell lines were grown in Euromed-N medium, supplemented with 10 ng/ml EGF, 10 ng/ml FGF2 and 1% N2 (Invitrogen Life Technologies). Floating tumor spheres with stem-like features were formed within 5-7 days and passaged every 10 days or once they reached 100-150 μm in size. 1 ml Euromed-N was added every 48 hours to the culture, to provide fresh medium to cells. Melanosphere conditioned medium was centrifuged to eliminate single cells and collected to be used for subsequent assays, mixed with 70% fresh medium.

Measurement of mitochondrial mass and activity

A375 and WM115 adherent cells were plated at 1.5×10^5 cells/dish in 6-cm dishes. After 48 hours or following transfection or treatment, they were harvested, washed in PBS and incubated with MitoTracker Green FM or Orange CMTMRos (Invitrogen Life Technologies) 10 nM for 30 min. Melanospheres were mechanically disaggregated by pipetting to reach a single cell suspension and then processed as above. Flow cytometry analysis was performed through a Novocyte3000 instrument (ACEA Biosciences, San Diego, CA). Data were analyzed with Novoexpress software.

Measurement of oxygen consumption rate

Measurement of oxygen consumption rate was conducted by performing a Mito Stress Test (Agilent Technologies, Santa Clara, CA, USA), as described in [15,16]. Briefly, both A375 and WM115 adherent and melanosphere-derived cells were seeded at 5×10^4 cells/well in a 24-well Agilent Seahorse XF Cell Culture Microplate, and oxygen consumption rate was recorded at the basal level and after the sequential injections of 1 μM Oligomycin (ATP synthase inhibitor), 1 μM FCCP (uncoupling agent) and 0.5 μM of a mixture of Rotenone (complex I inhibitor) and Antimycin A (complex III inhibitor). Oxygen consumption rate was normalized for protein content, determined by bicinchoninic acid (BCA) assay.

Measurement of ATP synthesis

ATP synthesis was quantified by using an ATP assay kit (GeneTex, Alton Pkwy Irvine, CA, USA) and an EnSpire Multimode Plate reader (PerkinElmer, Milano, Italy), as described in [17].

Measurement of mitochondrial ROS production

A375 and WM115 adherent cells were plated at 1.5×10^5 cells/dish in 6-cm dishes. After 48 hours, they were harvested, washed in PBS and incubated with MitoSOX Red (Invitrogen Life Technologies) 5 μM for 10 min. Melanospheres were mechanically disaggregated by pipetting to reach a single cell suspension and then processed as above. Flow cytometry analysis was performed through a Novocyte3000 instrument. Data were analyzed with Novoexpress software.

Cell transfection

A375 and WM115 adherent cells were seeded at 5×10^4 cells/well in 6-well plates for 48 hours and then transfected by using Lipofectamine 3000 reagent (Invitrogen Life Technologies), according to manufacturer's instructions.

MTT viability assay

A375 and WM115 adherent cells were seeded at 3×10^4 cells/well in 24-well plates for 48 hours and then exposed to SR-18292 (12.5-200 μM) or vehicle for 72 hours. The medium was then changed with MTT solution (0.5 mg/mL) in RPMI without phenol red and FBS; cells were incubated at 37 °C for 30 min and violet precipitate was dissolved with isopropanol. Absorbance at 550 nm was measured through an EnSpire Multimode Plate reader.

Colony formation assay

After transfection or treatment, A375 and WM115 adherent cells were seeded (250–500 cells/well, depending on the cell type) in 6-well plates and then cultured for 7–10 days. Colonies were fixed with 70% methanol and stained with Crystal Violet 0.15%.

Migration assay

Migration assay was performed using transwell filters (8 μm pore size). After transfection or treatment, A375 and WM115 adherent cells (1×10^5 cells/well) were placed in the top chambers of a 24-well plate in FBS-free media, in which the bottom chambers were filled with complete media. After incubation for 24 hours at 37 °C, cells that migrated to the lower chamber were stained with DiffQuick staining kit (DADE, Dudingen, Switzerland) and counted.

Melanosphere formation assay

After transfection or treatment, A375 and WM115 adherent cells were seeded in 25-cm^2 flasks and incubated with proper media for 7 days to determine their spheroidogenic potential. Melanospheres were photographed and counted with Zeiss Axiovert 200 microscope with a 10×1.4 objective lens linked to a Coolsnap Es CCD camera.

Melanosphere propagation assay

After treatment, A375 and WM115 melanosphere-derived cells were seeded in 25-cm^2 flasks and incubated with proper media for 7 days to determine their spheroidogenic potential. Melanospheres were photographed and counted with Zeiss Axiovert 200 microscope with a 10×1.4 objective lens linked to a Coolsnap Es CCD camera.

Evaluation of ABCG2 enrichment

After transfection or treatment, A375 and WM115 adherent cells were seeded in 25-cm^2 flasks and incubated with proper media for 7 days to determine ABCG2 enrichment. Melanospheres were mechanically disaggregated by pipetting to reach a single cell suspension, washed in PBS and incubated with anti-ABCG2 antibody (1:500) for 30 min. Flow cytometry analysis was performed through a Novocyte3000 instrument. Data were analyzed with Novoexpress software.

Western blot analysis

A375 and WM115 adherent cells were plated at 5×10^5 cells/dish in 10-cm dishes, and after 48 hours they were harvested and lysed in RIPA buffer. Melanospheres were collected, and protein extracts were prepared as above. Protein preparations (20 μg) were then resolved on SDS-PAGE and transferred to a nitrocellulose membrane. Membranes were incubated with the specific primary antibodies. Detection was done by using horseradish peroxidase-conjugated secondary antibodies and enhanced chemiluminescence reagents. GAPDH was utilized as loading control.

Statistical analysis

Statistical analysis was performed with a statistic package (GraphPad Prism5, GraphPad Software San Diego, CA, USA). Data are represented as the mean ± SEM of three independent experiments. Differences between groups were assessed by t-test or Dunnett's test after one-way analysis of variance. A P value < 0.05 was considered statistically significant.

RESULTS

Melanoma SCs display increased mitochondrial biogenesis

By using a 3D sphere culture model, we have recently demonstrated that a subpopulation of ABCG2+ cells endowed with CSC traits, including an enrichment in pluripotent embryonic stem cell markers and an increase in invasive ability, *in vivo* aggressiveness and therapy escape, is present in human melanoma [14]. Herein, we employed MitoTracker Green FM, a fluorescent probe that enters mitochondria regardless of membrane potential, to investigate the metabolic features of A375 and WM115 CSCs. Intriguingly, we found that melanoma SC subset displays higher mitochondrial mass compared with non-stem cells (Fig. 1A), suggesting that a correlation might exists between cancer stemness and an altered mitochondrial content.

To validate the above findings, we next examined mitochondrial biogenesis in A375 and WM115 melanospheres. This process is a self-renewal mechanism, by which new mitochondria are generated from the ones already existing. Its master regulator is PGC1-α, whose activation promotes the transcription and subsequent translation of the mtDNA-encoded genes into various proteins, including 13 polypeptides essential for OXPHOS [24]. Remarkably, Western blot analysis showed an upregulation of PGC1-α in spheroids with respect to adherent cells (Fig. 1B). Moreover, in melanoma CSCs we observed an

overexpression of OXPHOS complexes (Fig. 1C). Collectively, these results confirm the strict link between enhanced mitochondrial mass and a stem-like phenotype.

Melanoma SCs exhibit an oxidative metabolism

Based on the observations reported above, we further evaluated the role of mitochondria in melanoma SC compartment. In A375 and WM115 spheroids a significantly higher mitochondrial membrane potential was measured by MitoTracker Orange CMTMRos staining (Fig. 2A). Similarly, Mito Stress Test, which provides respiratory parameters, indicated that melanospheres exhibit higher oxygen consumption rate than their naïve counterpart, both in basal and in FCCP (carbonylcyanide-4-(trifluoromethoxy) phenylhydrazone)-uncoupled conditions (Fig. 2B). In addition, the response to oligomycin A, which accounts for non-phosphorylating respiration, showed that mitochondrial respiration is coupled to increased ATP synthesis, as also demonstrated by a specific colorimetric assay (Fig. 2B and 3A). Finally, an enhanced production of mitochondrial superoxide, the predominant ROS generated by the electron transport chain, was highlighted in A375 and WM115 CSCs (Fig. 3B). Overall, these data support the hypothesis by which melanoma SCs are characterized by an oxidative profile and strongly rely on mitochondrial metabolism to propagate within the tumor mass.

PGC1-α is required to maintain melanoma stem-like features

As previously mentioned, PGC1-α-mediated mitochondrial biogenesis has recently emerged as a key process in determining CSC expansion in different malignancies, such as breast, pancreatic and bile duct cancer [9,18–21]. Since PGC1-α is expressed at higher levels in melanoma SCs, we tested the effects of its genetic knockdown on the intrinsic characteristics of A375 and WM115 adherent cells. As expected, silencing of this molecule (Fig. 4A) led to a significant decrease in both mitochondrial mass and activity (Fig. S1A, B). More importantly, it resulted in the suppression of melanoma stem-like properties, namely *in vitro* tumorigenic and migratory potential (Fig. 4B, C). Of note, these functional effects were accompanied by a significant reduction in spherogenicity and ABCG2 enrichment (Fig. 4D, E). Taken together, these findings prove that PGC1-α-driven mitochondrial biogenesis is required for the maintenance of melanoma stem-like features, highlighting once again the association between cancer stemness and an improved mitochondrial machinery.

Melanoma SCs can be eradicated by targeting their mitochondria

To obtain additional information about the impact of mitochondrial biogenesis on melanoma SCs, A375 and WM115 adherent cells were exposed to XCT790, an inhibitor of the ERRα/PGC1-α pathway, and SR-18292, which promotes PGC1-α acetylation and subsequent inactivation. Remarkably, treatment with both drugs dose-dependently reduced melanoma cell viability (Fig. 5A and 7A), decreasing both mitochondrial mass and activity (Fig. S2A, B and S3A, B). Moreover, pharmacological inhibition of PGC1-α led to the abrogation of cell clonogenic ability and invasion (Fig. 5B, C and 7B, C). Finally, blockage of melanosphere

formation/propagation and ABCG2+ cell proliferation was found (Fig. 6A-D and 8A-D), once again following mitochondrial dysfunction (Fig. S4A, B and S5A, B). These results identify PGC1-α as a relevant target in melanoma SCs, outlining the possibility of successfully eradicating these cells by disrupting their mitochondrial homeostasis.

DISCUSSION

Malignant melanoma is the most aggressive type of skin cancer. Despite the availability of several therapeutic options, it is characterized by large heterogeneity that allows cancer cells to survive to standard treatments. Thus, drug resistance and tumor relapse still represent a huge problem [22,23].

One of the main causes of cancer aggressiveness is the presence of CSCs in the tumor mass. CSCs are a rare subpopulation of the cell bulk, capable of both self-renewal and multipotent differentiation and thus believed to be endowed with tumor-initiating abilities. For these reasons, they are commonly involved in treatment escape and cancer recurrence [2]. In this setting, the identification of specific CSC traits could provide new targets for cancer therapy.

Herein, we investigated the metabolic implications of cancer stemness in A375 and WM115 human melanoma cells, by comparing 2D and 3D culture models.

First, by employing the fluorescent staining with MitoTracker Green FM, we analyzed the mitochondrial content in A375 and WM115 cell lines, demonstrating that ABCG2-enriched melanospheres are characterized by higher mitochondrial mass. Overall, these results are in line with previous observations highlighting the crucial role of mitochondria in conferring stem-like traits to glioma and glioblastoma cells [24,25]. Similarly, increased numbers of these organelles have been found to correlate with enhanced aldehyde dehydrogenase (ALDH) activity and an ESA+/CD24- phenotype in breast cancer, allowing the identification of specific stem-like subpopulations in both tumor cell lines and tissues [9]. Moreover, a cell side-population with high mitochondrial mass is dramatically expanded in head and neck carcinomas during the first phases of tumor development [26]. In this context, our findings not only support previous data about the centrality of mitochondria in tumor initiation but also indicate that enhanced mitochondrial content may represent a key CSC characteristic in melanoma.

Based on the above evidence, we next designed experiments to unravel druggable targets that are specifically activated in melanoma CSCs. Intriguingly, we found that A375 and WM115 spheroids exhibit higher levels of the mitochondrial biogenesis activator PGC1-α and of OXPHOS complexes compared with parental cells, mediating a metabolic switch characterized by increased mitochondrial membrane potential, oxygen consumption, ATP synthesis and ROS production. In accordance with our findings, enhanced mitochondrial biogenesis and OXPHOS have been detected in breast and pancreatic CSCs [18–20,27,28]. In addition, cholangiocarcinoma stem-like cells have been reported to preferentially use electron transport chain-derived ATP as a source of energy and to strongly depend on oxygen uptake for their growth [21]. More importantly, Roesch et al. have recently demonstrated that long-term treatment with various drugs leads to the selection of slow-cycling melanoma cells expressing high levels of the histone demethylase

JARID1B and of OXPHOS proteins [29]. Collectively, our results are consistent with the idea that an optimized mitochondrial machinery sustains CSC maintenance and expansion.

To validate the above mitochondrial phenotype not only as a stemness marker but also as a potential therapeutic target, we evaluated the response of A375 and WM115 cells to both genetic depletion and pharmacological inhibition of PGC1-α. Interestingly, in both cell cultures silencing of this protein led to a decrease in colony growth, migration, spherogenic ability and ABCG2 expression. Likewise, exposure of melanoma cells to XCT790 and SR-18292, two chemical inhibitors of PGC1-α signaling, resulted in a dose-dependent reduction in cell proliferation, followed by a significant suppression of *in vitro* tumorigenicity, invasion, sphere formation/propagation and ABCG2 enrichment. Remarkably, recent studies have shown that blocking mitochondrial biogenesis can effectively prevent the anchorage-independent survival and propagation of epithelial tumor-initiating cells [21,30]. Similar results were also obtained with doxycycline, tigecycline and azithromycin, three well-established antibiotics able to target mitochondrial protein translation [16,29–32]. Furthermore, several OXPHOS inhibitors, including metformin, phenformin and atovaquone, have shown promise in CSC elimination [33–36]. Finally, a mitochondria-based oncology platform, named MITO-ONC-RX, has been recently proposed for eradicating tumor-initiating cells, evidencing the importance of these organelles in determining CSC survival and proliferation [37]. To the best of our knowledge, this is the first study highlighting the possibility of successfully eliminating melanoma CSCs by targeting mitochondrial biogenesis. In this regard, it is worth emphasizing that the regulation and role of PGC1-α in cancer is not univocal, with different oncogenic and lineage-specific modules finely stimulating this protein to promote or dampen tumorigenesis and metastasis, even in the same malignancy [40–42]; hence, systematic evaluation of context-specific determinants is necessary not only to expand our understanding of PGC1-α function but also to define new pharmacological strategies [42].

In conclusion, melanoma CSCs showed high mitochondrial mass, accompanied by increased mitochondrial biogenesis and OXPHOS, indicating that the stem-like phenotype reflects a specific metabolic state characterized by an improved mitochondrial machinery. In line with this premise, blockage of PGC1-α pathway correlated with the complete abrogation of melanoma stemness traits. Thus, these results suggest that, in addition to standard approaches, it might be useful to target the above metabolic features in order to prevent tumor relapse.

ACKNOWLEDGEMENTS

This research was supported by MIUR Progetto di Eccellenza (Department of Pharmacological and Biomolecular Sciences "Rodolfo Paoletti", Università degli Studi di Milano, Milan, Italy). F.F. was supported by an AIRC Fellowship for Italy (till 31st March 2023) and Fondazione Umberto Veronesi (since 1st April 2023).

AUTHORS' CONTRIBUTIONS

Conceptualization: FF; Methodology and investigation: FF, CM, MA, ASR; Formal analysis: FF, CM, MA, ASR; Supervision and project administration: FF; Writing – original draft: FF; Writing – review and editing: FF, CM, MR, PL; Funding acquisition: PL; Revision and final approval: all authors revised and approved the manuscript.

DECLARATION OF COMPETING INTEREST

The authors declare no conflict of interest.

REFERENCES

[1] M. Marzagalli, M. Raimondi, F. Fontana, M. Montagnani Marelli, R.M. Moretti, P. Limonta, Cellular and molecular biology of cancer stem cells in melanoma: Possible therapeutic implications, Semin. Cancer Biol. 59 (2019) 221–235. doi:10.1016/j.semcancer.2019.06.019.

[2] M. Marzagalli, F. Fontana, M. Raimondi, P. Limonta, Cancer Stem Cells—Key Players in Tumor Relapse, Cancers (Basel). 13 (2021) 376. doi:10.3390/cancers13030376.

[3] M. Anselmi, F. Fontana, M. Marzagalli, N. Gagliano, M. Sommariva, P. Limonta, Melanoma Stem Cells Educate Neutrophils to Support Cancer Progression, Cancers (Basel). 14 (2022) 3391. doi:10.3390/cancers14143391.

[4] T.M. Ashton, W.G. McKenna, L.A. Kunz-Schughart, G.S. Higgins, Oxidative Phosphorylation as an Emerging Target in Cancer Therapy, Clin. Cancer Res. 24 (2018) 2482–2490. doi:10.1158/1078-0432.CCR-17-3070.

[5] F. Fontana, M. Raimondi, M. Marzagalli, M. Audano, G. Beretta, P. Procacci, P. Sartori, N. Mitro, P. Limonta, Mitochondrial functional and structural impairment is involved in the antitumor activity of δ-tocotrienol in prostate cancer cells, Free Radic. Biol. Med. (2020). doi:10.1016/j.freeradbiomed.2020.07.009.

[6] M. Raimondi, F. Fontana, M. Marzagalli, M. Audano, G. Beretta, P. Procacci, P. Sartori, N. Mitro, P. Limonta, Ca2+ overload- and ROS-associated mitochondrial dysfunction contributes to δ-tocotrienol-mediated paraptosis in melanoma cells, Apoptosis. (2021). doi:10.1007/s10495-021-01668-y.

[7] R. Lamb, H. Harrison, J. Hulit, D.L. Smith, M.P. Lisanti, F. Sotgia, Mitochondria as new therapeutic targets for eradicating cancer stem cells: Quantitative proteomics and functional validation via MCT1/2 inhibition, Oncotarget. 5 (2014) 11029–11037. doi:10.18632/oncotarget.2789.

[8] R. Lamb, B. Ozsvari, C.L. Lisanti, H.B. Tanowitz, A. Howell, U.E. Martinez-Outschoorn, F. Sotgia,

M.P. Lisanti, Antibiotics that target mitochondria effectively eradicate cancer stem cells, across multiple tumor types: Treating cancer like an infectious disease, Oncotarget. 6 (2015) 4569–4584. doi:10.18632/oncotarget.3174.

[9] G. Farnie, F. Sotgia, M.P. Lisanti, High mitochondrial mass identifies a sub-population of stem-like cancer cells that are chemo-resistant, Oncotarget. 6 (2015) 30472–30486. doi:10.18632/oncotarget.5401.

[10] R. Lamb, G. Bonuccelli, B. Ozsvári, M. Peiris-Pagès, M. Fiorillo, D.L. Smith, G. Bevilacqua, C.M. Mazzanti, L.A. McDonnell, A.G. Naccarato, M. Chiu, L. Wynne, U.E. Martinez-Outschoorn, F. Sotgia, M.P. Lisanti, Mitochondrial mass, a new metabolic biomarker for stem-like cancer cells: Understanding WNT/FGF-driven anabolic signaling, Oncotarget. 6 (2015) 30453–30471. doi:10.18632/oncotarget.5852.

[11] E.M. De Francesco, F. Sotgia, M.P. Lisanti, Cancer stem cells (CSCs): metabolic strategies for their identification and eradication, Biochem. J. 475 (2018) 1611–1634. doi:10.1042/BCJ20170164.

[12] F. Sotgia, M. Fiorillo, M.P. Lisanti, Hallmarks of the cancer cell of origin: Comparisons with "energetic" cancer stem cells (e-CSCs), Aging (Albany. NY). 11 (2019) 1065–1068. doi:10.18632/aging.101822.

[13] M. Fiorillo, F. Sotgia, M.P. Lisanti, "Energetic" Cancer Stem Cells (e-CSCs): A New Hyper-Metabolic and Proliferative Tumor Cell Phenotype, Driven by Mitochondrial Energy, Front. Oncol. 8 (2019). doi:10.3389/fonc.2018.00677.

[14] M. Marzagalli, R.M. Moretti, E. Messi, M.M. Marelli, F. Fontana, A. Anastasia, M.R. Bani, G. Beretta, P. Limonta, Targeting melanoma stem cells with the Vitamin E derivative δ-tocotrienol., Sci. Rep. 8 (2018) 587. doi:10.1038/s41598-017-19057-4.

[15] C. Macchi, A. Moregola, M.F. Greco, M. Svecla, F. Bonacina, S. Dhup, R.K. Dadhich, M. Audano, P. Sonveaux, C. Mauro, N. Mitro, M. Ruscica, G.D. Norata, Monocarboxylate transporter 1 deficiency impacts CD8+ T lymphocytes proliferation and recruitment to adipose tissue during obesity, IScience. 25 (2022) 104435. doi:10.1016/j.isci.2022.104435.

[16] C. Macchi, V. Bonalume, M.F. Greco, M. Mozzo, V. Melfi, C.R. Sirtori, V. Magnaghi, A. Corsini, M. Ruscica, Impact of Atorvastatin on Skeletal Muscle Mitochondrial Activity, Locomotion and Axonal Excitability—Evidence from ApoE-/- Mice, Int. J. Mol. Sci. 23 (2022) 5415. doi:10.3390/ijms23105415.

[17] F. Fontana, M. Anselmi, P. Limonta, Exploiting the Metabolic Consequences of PTEN Loss and Akt/Hexokinase 2 Hyperactivation in Prostate Cancer: A New Role for δ-Tocotrienol, Int. J. Mol. Sci. 23 (2022) 5269. doi:10.3390/ijms23095269.

[18] R. Sánchez-Alvarez, E.M. De Francesco, M. Fiorillo, F. Sotgia, M.P. Lisanti, Mitochondrial Fission Factor (MFF) Inhibits Mitochondrial Metabolism and Reduces Breast Cancer Stem Cell (CSC) Activity, Front. Oncol. 10 (2020). doi:10.3389/fonc.2020.01776.

[19] P. Sancho, E. Burgos-Ramos, A. Tavera, T. Bou Kheir, P. Jagust, M. Schoenhals, D. Barneda, K. Sellers, R. Campos-Olivas, O. Graña, C.R. Viera, M. Yuneva, B. Sainz, C. Heeschen, MYC/PGC-1α Balance Determines the Metabolic Phenotype and Plasticity of Pancreatic Cancer Stem Cells, Cell Metab. 22 (2015) 590–605. doi:10.1016/j.cmet.2015.08.015.

[20] A. Viale, P. Pettazzoni, C.A. Lyssiotis, H. Ying, N. Sánchez, M. Marchesini, A. Carugo, T. Green, S. Seth, V. Giuliani, M. Kost-Alimova, F. Muller, S. Colla, L. Nezi, G. Genovese, A.K. Deem, A. Kapoor, W. Yao, E. Brunetto, Y. Kang, M. Yuan, J.M. Asara, Y.A. Wang, T.P. Heffernan, A.C. Kimmelman, H. Wang, J.B. Fleming, L.C. Cantley, R.A. DePinho, G.F. Draetta, Oncogene ablation-resistant pancreatic cancer cells depend on mitochondrial function, Nature. 514 (2014) 628–632. doi:10.1038/nature13611.

[21] C. Raggi, M.L. Taddei, E. Sacco, N. Navari, M. Correnti, B. Piombanti, M. Pastore, C. Campani, E. Pranzini, J. Iorio, G. Lori, T. Lottini, C. Pearce, J. Cibella, M. Lewinska, J.B. Andersen, L. di Tommaso, L. Viganò, G. Di Maira, S. Madiai, M. Ramazzotti, I. Orlandi, A. Arcangeli, P. Chiarugi, F. Marra, Mitochondrial oxidative metabolism contributes to a cancer stem cell phenotype in cholangiocarcinoma, J. Hepatol. 74 (2021) 1373–1385. doi:10.1016/j.jhep.2020.12.031.

[22] A. Millet, A.R. Martin, C. Ronco, S. Rocchi, R. Benhida, Metastatic Melanoma: Insights Into the Evolution of the Treatments and Future Challenges, Med. Res. Rev. 37 (2017) 98–148. doi:10.1002/med.21404.

[23] H. Patel, N. Yacoub, R. Mishra, A. White, L. Yuan, S. Alanazi, J.T. Garrett, Current Advances in the Treatment of BRAF-Mutant Melanoma, Cancers (Basel). 12 (2020) 482. doi:10.3390/cancers12020482.

[24] S. Yuan, Y. Lu, J. Yang, G. Chen, S. Kim, L. Feng, M. Ogasawara, N. Hammoudi, W. Lu, H. Zhang, J. Liu, H. Colman, J.-S. Lee, X.-N. Li, R. Xu, P. Huang, F. Wang, Metabolic activation of mitochondria in glioma stem cells promotes cancer development through a reactive oxygen species-mediated mechanism, Stem Cell Res. Ther. 6 (2015) 198. doi:10.1186/s13287-015-0174-2.

[25] Y. Iranmanesh, B. Jiang, O.C. Favour, Z. Dou, J. Wu, J. Li, C. Sun, Mitochondria's Role in the Maintenance of Cancer Stem Cells in Glioblastoma, Front. Oncol. 11 (2021). doi:10.3389/fonc.2021.582694.

[26] J.M. Curry, M. Tuluc, D. Whitaker-Menezes, J.A. Ames, A. Anantharaman, A. Butera, B. Leiby, D. Cognetti, F. Sotgia, M.P. Lisanti, U.E. Martinez-Outschoorn, Cancer metabolism, stemness and tumor recurrence, Cell Cycle. 12 (2013) 1371–1384. doi:10.4161/cc.24092.

[27] K. Lee, J.M. Giltnane, J.M. Balko, L.J. Schwarz, A.L. Guerrero-Zotano, K.E. Hutchinson, M.J. Nixon, M. V. Estrada, V. Sánchez, M.E. Sanders, T. Lee, H. Gómez, A. Lluch, J.A. Pérez-Fidalgo, M.M. Wolf, G. Andrejeva, J.C. Rathmell, S.W. Fesik, C.L. Arteaga, MYC and MCL1 Cooperatively Promote Chemotherapy-Resistant Breast Cancer Stem Cells via Regulation of Mitochondrial Oxidative Phosphorylation, Cell Metab. 26 (2017) 633-647.e7. doi:10.1016/j.cmet.2017.09.009.

[28] S. Valle, S. Alcalá, L. Martin-Hijano, P. Cabezas-Sáinz, D. Navarro, E.R. Muñoz, L. Yuste, K. Tiwary, K. Walter, L. Ruiz-Cañas, M. Alonso-Nocelo, J.A. Rubiolo, E. González-Arnay, C. Heeschen, L. Garcia-Bermejo, P.C. Hermann, L. Sánchez, P. Sancho, M.Á. Fernández-Moreno, B. Sainz, Exploiting oxidative phosphorylation to promote the stem and immunoevasive properties of pancreatic cancer stem cells, Nat. Commun. 11 (2020) 5265. doi:10.1038/s41467-020-18954-z.

[29] A. Roesch, A. Vultur, I. Bogeski, H. Wang, K.M. Zimmermann, D. Speicher, C. Körbel, M.W. Laschke, P.A. Gimotty, S.E. Philipp, E. Krause, S. Pätzold, J. Villanueva, C. Krepler, M. Fukunaga-Kalabis, M. Hoth, B.C. Bastian, T. Vogt, M. Herlyn, Overcoming Intrinsic Multidrug Resistance in Melanoma by Blocking the Mitochondrial Respiratory Chain of Slow-Cycling JARID1Bhigh Cells, Cancer Cell. 23 (2013) 811–825. doi:10.1016/j.ccr.2013.05.003.

[30] A. De Luca, M. Fiorillo, M. Peiris-Pagès, B. Ozsvari, D.L. Smith, R. Sanchez-Alvarez, U.E. Martinez-Outschoorn, A.R. Cappello, V. Pezzi, M.P. Lisanti, F. Sotgia, Mitochondrial biogenesis is required for the anchorage-independent survival and propagation of stem-like cancer cells, Oncotarget. 6 (2015) 14777–14795. doi:10.18632/oncotarget.4401.

[31] E.M. De Francesco, M. Maggiolini, H.B. Tanowitz, F. Sotgia, M.P. Lisanti, Targeting hypoxic cancer stem cells (CSCs) with Doxycycline: Implications for optimizing anti-angiogenic therapy, Oncotarget. 8 (2017) 56126–56142. doi:10.18632/oncotarget.18445.

[32] L. Zhang, L. Xu, F. Zhang, E. Vlashi, Doxycycline inhibits the cancer stem cell phenotype and epithelial-to-mesenchymal transition in breast cancer, Cell Cycle. 16 (2017) 737–745. doi:10.1080/15384101.2016.1241929.

[33] C. Scatena, M. Roncella, A. Di Paolo, P. Aretini, M. Menicagli, G. Fanelli, C. Marini, C.M. Mazzanti, M. Ghilli, F. Sotgia, M.P. Lisanti, A.G. Naccarato, Doxycycline, an Inhibitor of Mitochondrial Biogenesis, Effectively Reduces Cancer Stem Cells (CSCs) in Early Breast Cancer Patients: A Clinical Pilot Study, Front. Oncol. 8 (2018). doi:10.3389/fonc.2018.00452.

[34] D.J. Chu, D.E. Yao, Y.F. Zhuang, Y. Hong, X.C. Zhu, Z.R. Fang, J. Yu, Z.Y. Yu, Azithromycin enhances the favorable results of paclitaxel and cisplatin in patients with advanced non-small cell lung cancer, Genet. Mol. Res. 13 (2014) 2796–2805. doi:10.4238/2014.April.14.8.

[35] H.A. Hirsch, D. Iliopoulos, P.N. Tsichlis, K. Struhl, Metformin Selectively Targets Cancer Stem Cells, and Acts Together with Chemotherapy to Block Tumor Growth and Prolong Remission,

Cancer Res. 69 (2009) 7507–7511. doi:10.1158/0008-5472.CAN-09-2994.

[36] E. Lonardo, M. Cioffi, P. Sancho, Y. Sanchez-Ripoll, S.M. Trabulo, J. Dorado, A. Balic, M. Hidalgo, C. Heeschen, Metformin Targets the Metabolic Achilles Heel of Human Pancreatic Cancer Stem Cells, PLoS One. 8 (2013) e76518. doi:10.1371/journal.pone.0076518.

[37] J. Park, J.-K. Shim, J.H. Kang, J. Choi, J.H. Chang, S.-Y. Kim, S.-G. Kang, Regulation of bioenergetics through dual inhibition of aldehyde dehydrogenase and mitochondrial complex I suppresses glioblastoma tumorspheres, Neuro. Oncol. 20 (2018) 954–965. doi:10.1093/neuonc/nox243.

[38] M. Fiorillo, R. Lamb, H.B. Tanowitz, L. Mutti, M. Krstic-Demonacos, A.R. Cappello, U.E. Martinez-Outschoorn, F. Sotgia, M.P. Lisanti, Repurposing atovaquone: Targeting mitochondrial complex III and OXPHOS to eradicate cancer stem cells, Oncotarget. 7 (2016) 34084–34099. doi:10.18632/oncotarget.9122.

[39] F. Sotgia, B. Ozsvari, M. Fiorillo, E.M. De Francesco, G. Bonuccelli, M.P. Lisanti, A mitochondrial based oncology platform for targeting cancer stem cells (CSCs): MITO-ONC-RX, Cell Cycle. 17 (2018) 2091–2100. doi:10.1080/15384101.2018.1515551.

[40] C. Luo, J.-H. Lim, Y. Lee, S.R. Granter, A. Thomas, F. Vazquez, H.R. Widlund, P. Puigserver, A PGC1α-mediated transcriptional axis suppresses melanoma metastasis, Nature. 537 (2016) 422–426. doi:10.1038/nature19347.

[41] F. Vazquez, J.-H. Lim, H. Chim, K. Bhalla, G. Girnun, K. Pierce, C.B. Clish, S.R. Granter, H.R. Widlund, B.M. Spiegelman, P. Puigserver, PGC1α Expression Defines a Subset of Human Melanoma Tumors with Increased Mitochondrial Capacity and Resistance to Oxidative Stress, Cancer Cell. 23 (2013) 287–301. doi:10.1016/j.ccr.2012.11.020.

[42] S.-P. Gravel, Deciphering the Dichotomous Effects of PGC-1α on Tumorigenesis and Metastasis, Front. Oncol. 8 (2018). doi:10.3389/fonc.2018.00075.

FIGURE CAPTIONS

Fig. 1. Melanoma SCs display increased mitochondrial biogenesis. A, Mitochondrial mass was measured in A375 and WM115 adherent and melanosphere-derived cells by flow cytometry. Each experiment was repeated three times. Data represent mean values ± SEM and were analyzed by t-test. ***P < 0.001 vs A375 or WM115. **B**, PGC1-α expression was analyzed in A375 and WM115 adherent and melanosphere-derived cells by Western blot analysis. GAPDH expression was evaluated as a loading control. One representative of three experiments performed is shown. **B**, OXPHOS complex expression was analyzed in A375 and WM115

adherent and melanosphere-derived cells by Western blot analysis. GAPDH expression was evaluated as a loading control. One representative of three experiments performed is shown.

Fig. 2. Melanoma SCs exhibit enhanced mitochondrial activity and oxygen consumption rate. A, Mitochondrial activity was measured in A375 and WM115 adherent and melanosphere-derived cells by flow cytometry. Each experiment was repeated three times. Data represent mean values ± SEM and were analyzed by t-test. ***P < 0.001 vs A375 or WM115. **B**, Oxygen consumption rate was evaluated in A375 and WM115 adherent and melanosphere-derived cells by Mito Stress Test. Each experiment was repeated three times. Data represent mean values ± SEM and were analyzed by t-test. *P < 0.05 vs A375 or WM115. **P < 0.01 vs A375 or WM115.

Fig. 3. ATP synthesis and mitochondrial ROS production are higher in melanoma SCs. A, ATP synthesis mas evaluated in A375 and WM115 adherent and melanosphere-derived cells by colorimetric assay. Each experiment was repeated three times. Data represent mean values ± SEM and were analyzed by t-test. *P < 0.05 vs A375 or WM115. **P < 0.01 vs A375 or WM115. **B**, Mitochondrial ROS production was measured in A375 and WM115 adherent and melanosphere-derived cells by flow cytometry. Each experiment was repeated three times. Data represent mean values ± SEM and were analyzed by t-test. ***P < 0.001 vs A375 or WM115.

Fig. 4. PGC1-α is required to maintain melanoma stem-like features. A, After transfection, PGC1-α expression was analyzed in A375 and WM115 adherent cells by Western blot analysis. GAPDH expression was evaluated as a loading control. One representative of three experiments performed is shown. **B**, After transfection, clonogenic ability was evaluated in A375 and WM115 adherent cells by colony formation assay. Each experiment was repeated three times. Data represent mean values ± SEM and were analyzed by t-test. **P < 0.01 vs Scramble. **C**, After transfection, invasive potential was evaluated in A375 and WM115 adherent cells by transwell migration assay. Each experiment was repeated three times. Data represent mean values ± SEM and were analyzed by t-test. *P < 0.05 vs Scramble. **D**, After transfection, spherogenic ability was evaluated in A375 and WM115 adherent cells by sphere formation assay. Each experiment was repeated three times. Data represent mean values ± SEM and were analyzed by t-test. *P < 0.05 vs Scramble. **E**, After transfection, ABCG2 enrichment was measured in A375 and WM115 adherent cells by flow cytometry. Each experiment was repeated three times. Data represent mean values ± SEM and were analyzed by t-test. **P < 0.01 vs Scramble. ***P < 0.001 vs Scramble.

Fig. 5. XCT790 decreases melanoma cell viability, colony formation and migration. A, A375 and WM115 adherent cells with XCT790 (1.5-20 μM) for 48 hours. Cell viability was then evaluated by MTT assay. Each experiment was repeated three times. Data represent mean values ± SEM and were analyzed by Dunnet's test after one-way analysis of variance. **P < 0.01 vs 0, controls (vehicle); ***P < 0.001 vs 0, controls (vehicle). **B**, A375 and WM115 adherent cells with XCT790 (10 μM) for 48 hours. Clonogenic ability was evaluated by colony formation assay. Each experiment was repeated three times. Data represent mean values ± SEM and were analyzed by t-test. ***P < 0.001 vs C, controls (vehicle). **C**, A375 and

WM115 adherent cells with XCT790 (10 μM) for 48 hours. Invasive potential was evaluated by transwell migration assay. Each experiment was repeated three times. Data represent mean values ± SEM and were analyzed by t-test. *P < 0.05 vs C, controls (vehicle).

Fig. 6. XCT790 suppresses melanoma cell spherogenic ability and ABCG2 enrichment. A, A375 and WM115 adherent cells with XCT790 (10 μM) for 48 hours. Spherogenic ability was then evaluated by sphere formation assay. Data represent mean values ± SEM and were analyzed by t-test. **P < 0.05 vs C, controls (vehicle). **B**, A375 and WM115 adherent cells with XCT790 (10 μM) for 48 hours. ABCG2 enrichment was then measured by flow cytometry. Each experiment was repeated three times. Data represent mean values ± SEM and were analyzed by t-test. *P < 0.05 vs C, controls (vehicle). **P < 0.01 vs C, controls (vehicle). **C**, A375 and WM115 melanosphere-derived cells with XCT790 (10 μM) for 48 hours. Invasive potential was evaluated by transwell migration assay. Each experiment was repeated three times. Data represent mean values ± SEM and were analyzed by t-test. **P < 0.01 vs C, controls (vehicle). **D**, A375 and WM115 melanosphere-derived cells with XCT790 (10 μM) for 48 hours. ABCG2 enrichment was then measured by flow cytometry. Each experiment was repeated three times. Data represent mean values ± SEM and were analyzed by t-test. *P < 0.05 vs C, controls (vehicle). **P < 0.01 vs C, controls (vehicle).

Fig. 7. SR-18292 decreases melanoma cell viability, colony formation and migration. A, A375 and WM115 adherent cells with SR-18292 (12.5-200 μM) for 48 hours. Cell viability was then evaluated by MTT assay. Each experiment was repeated three times. Data represent mean values ± SEM and were analyzed by Dunnet's test after one-way analysis of variance. ***P < 0.001 vs 0, controls (vehicle). **B**, A375 and WM115 adherent cells with SR-18292 (50 μM) for 48 hours. Clonogenic ability was evaluated by colony formation assay. Each experiment was repeated three times. Data represent mean values ± SEM and were analyzed by t-test. ***P < 0.001 vs C, controls (vehicle). **C**, A375 and WM115 adherent cells with SR-18292 (50 μM) for 48 hours. Invasive potential was evaluated by transwell migration assay. Each experiment was repeated three times. Data represent mean values ± SEM and were analyzed by t-test. *P < 0.05 vs C, controls (vehicle). **P < 0.01 vs C, controls (vehicle).

Fig. 8. SR-18292 suppresses melanoma cell spherogenic ability and ABCG2 enrichment. A, A375 and WM115 adherent cells with SR-18292 (50 μM) for 48 hours. Spherogenic ability was then evaluated by sphere formation assay. Data represent mean values ± SEM and were analyzed by t-test. ***P < 0.001 vs C, controls (vehicle). **B**, A375 and WM115 adherent cells with SR-18292 (50 μM) for 48 hours. ABCG2 enrichment was then measured by flow cytometry. Each experiment was repeated three times. Data represent mean values ± SEM and were analyzed by t-test. ***P < 0.001 vs C, controls (vehicle). **C**, A375 and WM115 melanosphere-derived cells with SR-18292 (50 μM) for 48 hours. Invasive potential was evaluated by transwell migration assay. Each experiment was repeated three times. Data represent mean values ± SEM and were analyzed by t-test. ***P < 0.001 vs C, controls (vehicle). **D**, A375 and WM115 melanosphere-derived cells with SR-18292 (50 μM) for 48 hours. ABCG2 enrichment was then measured by flow

cytometry. Each experiment was repeated three times. Data represent mean values ± SEM and were analyzed by t-test. ***P < 0.001 vs C, controls (vehicle).

Suppl Fig 1. PGC1-α silencing leads to a reduction in mitochondrial mass and activity. A, After transfection, mitochondrial mass was measured in A375 and WM115 cells by flow cytometry. Each experiment was repeated three times. Data represent mean values ± SEM and were analyzed by t-test. ***P < 0.001 vs Scramble. **B**, After transfection, mitochondrial activity was measured in A375 and WM115 cells by flow cytometry. Each experiment was repeated three times. Data represent mean values ± SEM and were analyzed by t-test. ***P < 0.001 vs Scramble.

Suppl Fig 2. XCT790 reduces mitochondrial mass and activity in melanoma cells. A, After treatment, mitochondrial mass was measured in A375 and WM115 cells by flow cytometry. Each experiment was repeated three times. Data represent mean values ± SEM and were analyzed by t-test. ***P < 0.001 vs C, controls (vehicle). **B**, After treatment, mitochondrial activity was measured in A375 and WM115 cells by flow cytometry. Each experiment was repeated three times. Data represent mean values ± SEM and were analyzed by t-test. ***P < 0.001 vs C, controls (vehicle).

Suppl Fig 3. SR-18292 reduces mitochondrial mass and activity in melanoma cells. A, After treatment, mitochondrial mass was measured in A375 and WM115 cells by flow cytometry. Each experiment was repeated three times. Data represent mean values ± SEM and were analyzed by t-test. ***P < 0.001 vs C, controls (vehicle). **B**, After treatment, mitochondrial activity was measured in A375 and WM115 cells by flow cytometry. Each experiment was repeated three times. Data represent mean values ± SEM and were analyzed by t-test. ***P < 0.001 vs C, controls (vehicle).

Suppl Fig 4. XCT790 reduces mitochondrial mass and activity in melanosphere-derived cells. A, After treatment, mitochondrial mass was measured in A375 and WM115 melanosphere-derived cells by flow cytometry. Each experiment was repeated three times. Data represent mean values ± SEM and were analyzed by t-test. ***P < 0.001 vs C, controls (vehicle). **B**, After treatment, mitochondrial activity was measured in A375 and WM115 melanosphere-derived cells by flow cytometry. Each experiment was repeated three times. Data represent mean values ± SEM and were analyzed by t-test. ***P < 0.001 vs C, controls (vehicle).

Suppl Fig 5. SR-18292 reduces mitochondrial mass and activity in melanosphere-derived cells. A, After treatment, mitochondrial mass was measured in A375 and WM115 melanosphere-derived cells by flow cytometry. Each experiment was repeated three times. Data represent mean values ± SEM and were analyzed by t-test. ***P < 0.001 vs C, controls (vehicle). **B**, After treatment, mitochondrial activity was measured in A375 and WM115 melanosphere-derived cells by flow cytometry. Each experiment was repeated three times. Data represent mean values ± SEM and were analyzed by t-test. ***P < 0.001 vs C, controls (vehicle).

HIGHLIGHTS

- Melanoma stem cells exhibit increased mitochondrial mass
- This correlates with enhanced mitochondrial biogenesis and oxidative phosphorylation
- Inhibition of PGC1-α pathway leads to melanoma stem cell eradication

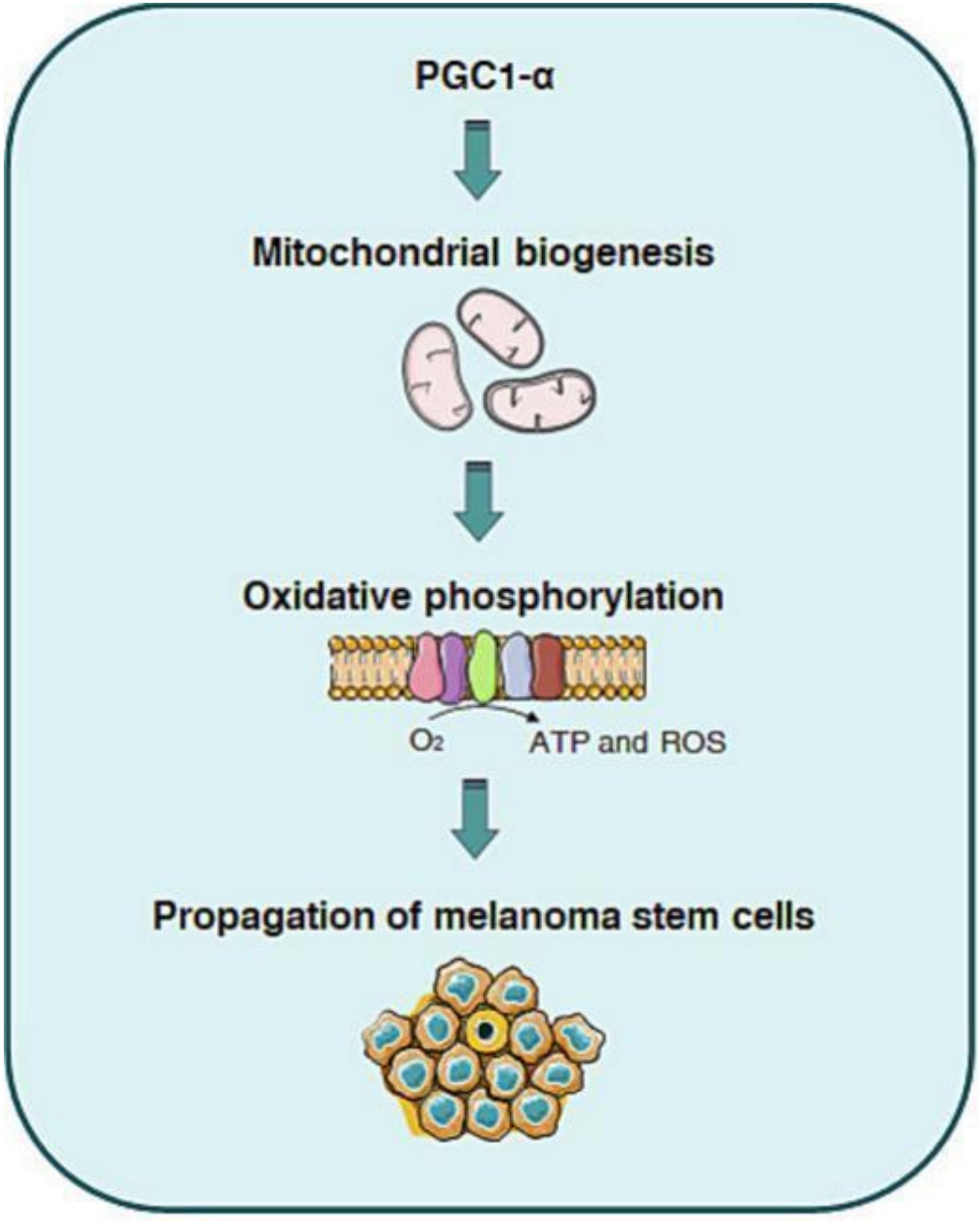

Graphics Abstract

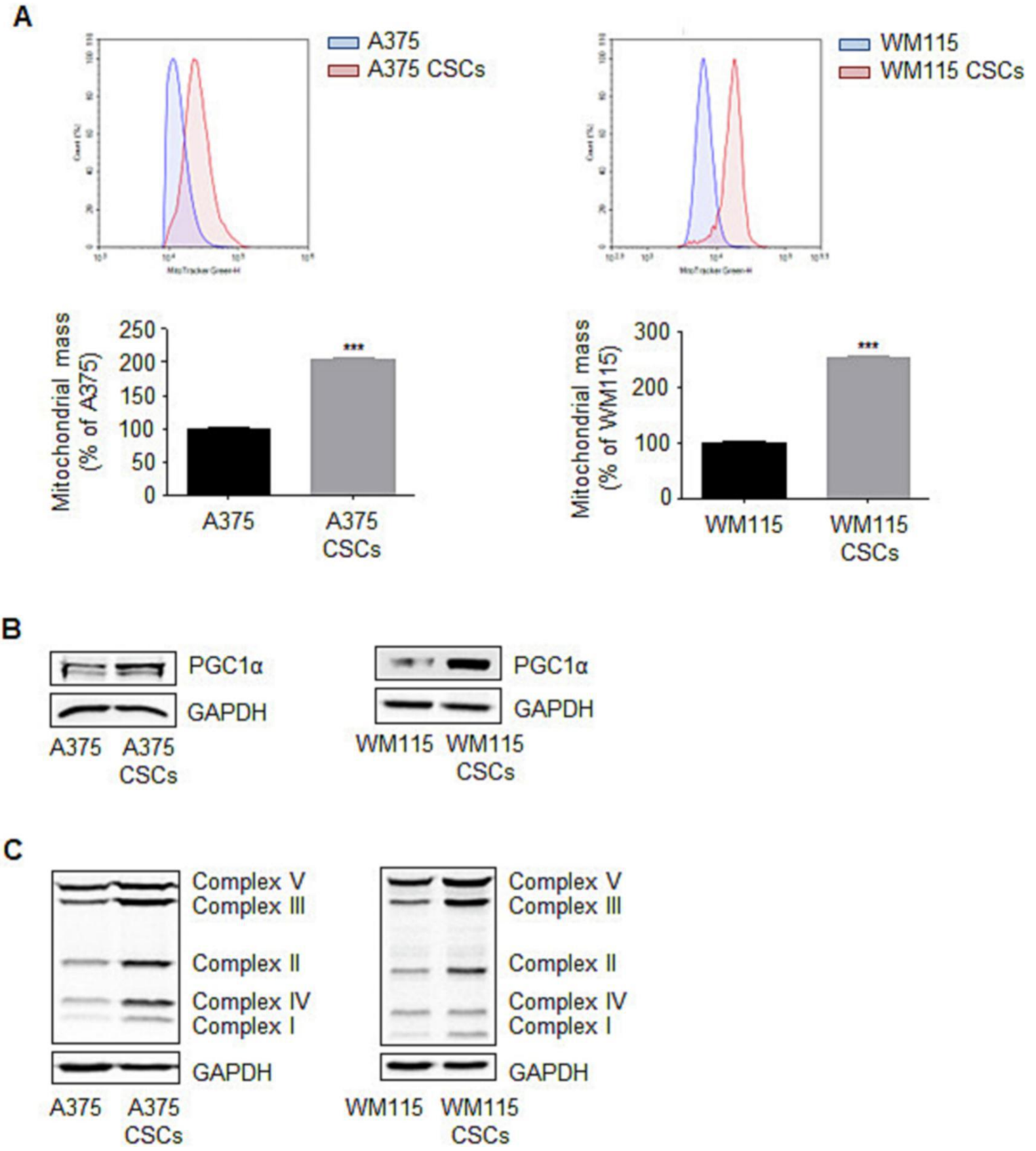
A
A375
A375 CSCs
WM115
WM115 CSCs
Mitochondrial mass (% of A375)
250
200
150
100
50
0
***
A375
A375 CSCs
Mitochondrial mass (% of WM115)
300
200
100
0
***
WM115
WM115 CSCs
B
PGC1α
GAPDH
A375
A375 CSCs
PGC1α
GAPDH
WM115
WM115 CSCs
C
Complex V
Complex III
Complex II
Complex IV
Complex I
GAPDH
A375
A375 CSCs
Complex V
Complex III
Complex II
Complex IV
Complex I
GAPDH
WM115
WM115 CSCs

Figure 1

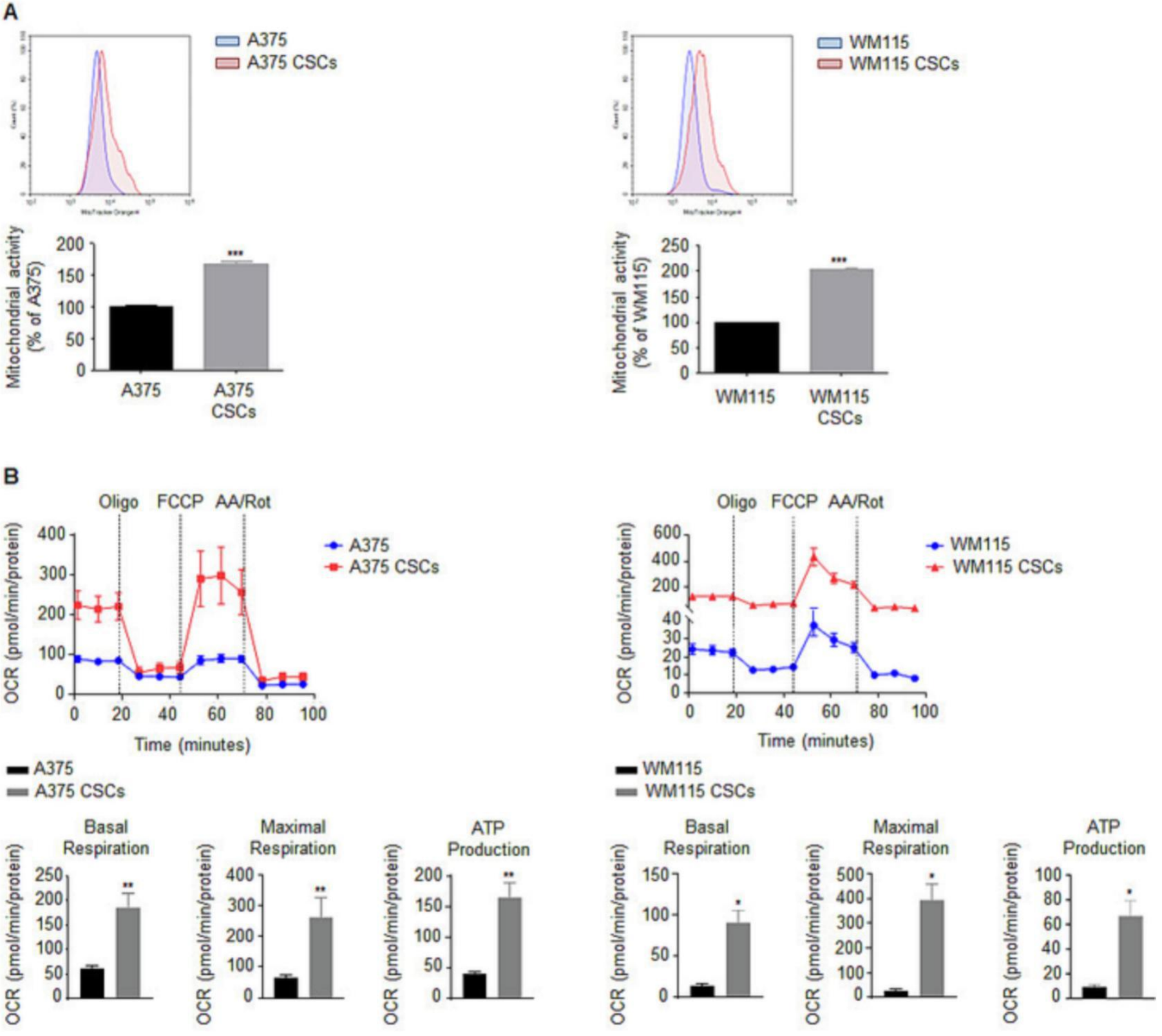
A
A375
A375 CSCs
WM115
WM115 CSCs
Mitochondrial activity (% of A375)
Mitochondrial activity (% of WM115)
A375
A375 CSCs
WM115
WM115 CSCs
B
Oligo
FCCP
AA/Rot
OCR (pmol/min/protein)
Time (minutes)
Basal Respiration
Maximal Respiration
ATP Production

Figure 2

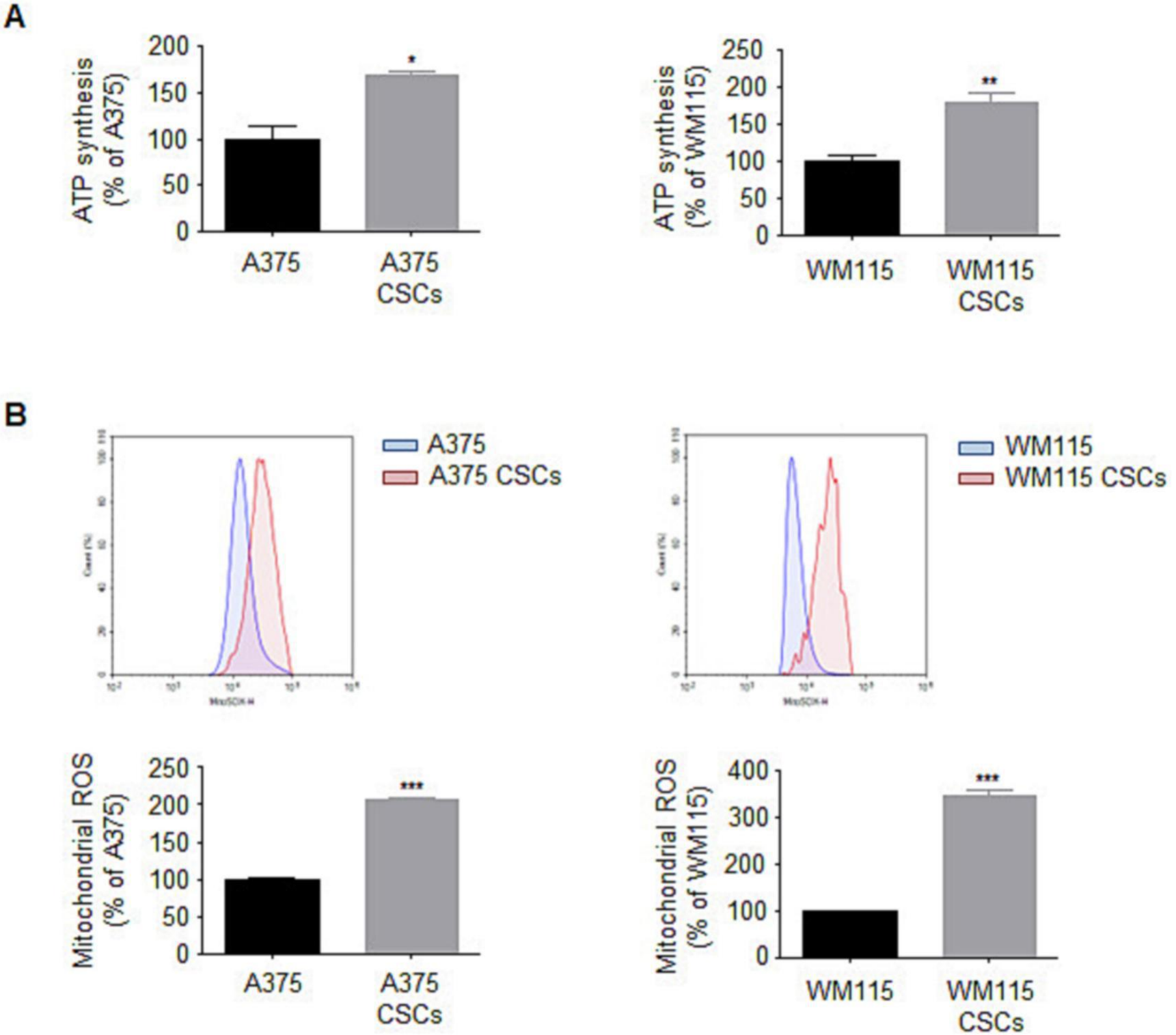
A
ATP synthesis (% of A375)
200
150
100
50
0
*
A375
A375 CSCs
ATP synthesis (% of WM115)
250
200
150
100
50
0
**
WM115
WM115 CSCs
B
A375
A375 CSCs
WM115
WM115 CSCs
Mitochondrial ROS (% of A375)
250
200
150
100
50
0
***
A375
A375 CSCs
Mitochondrial ROS (% of WM115)
400
300
200
100
0
***
WM115
WM115 CSCs

Figure 3

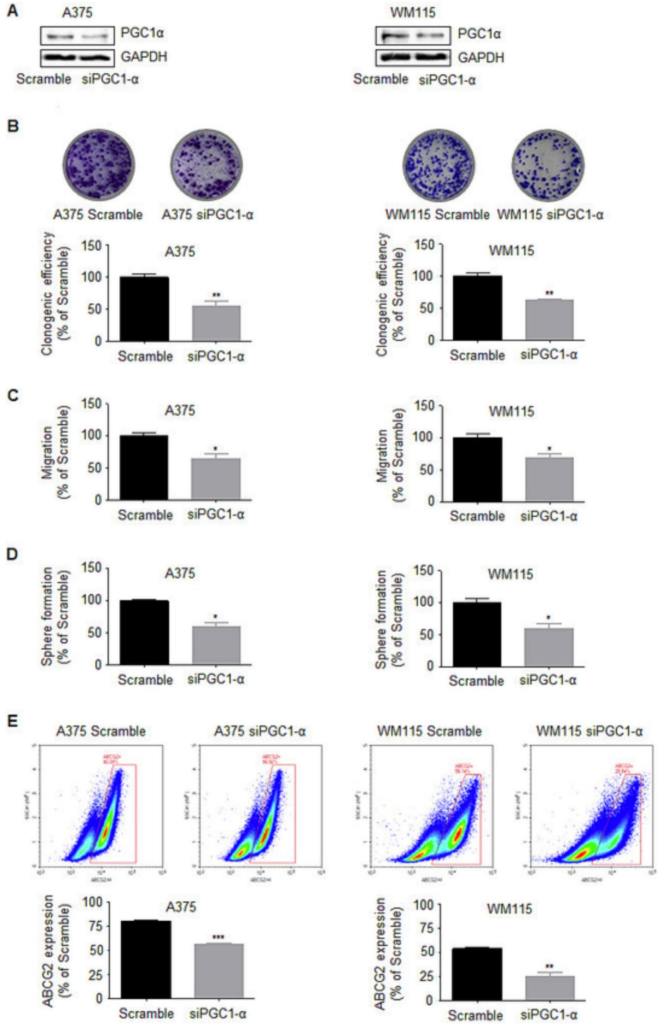
A
A375
PGC1α
GAPDH
Scramble siPGC1-α
WM115
PGC1α
GAPDH
Scramble siPGC1-α
B
A375 Scramble
A375 siPGC1-α
WM115 Scramble
WM115 siPGC1-α
Clonogenic efficiency (% of Scramble)
A375
WM115
Scramble
siPGC1-α
C
Migration (% of Scramble)
A375
WM115
Scramble
siPGC1-α
D
Sphere formation (% of Scramble)
A375
WM115
Scramble
siPGC1-α
E
A375 Scramble
A375 siPGC1-α
WM115 Scramble
WM115 siPGC1-α
ABCG2 expression (% of Scramble)
A375
WM115
Scramble
siPGC1-α

Figure 4

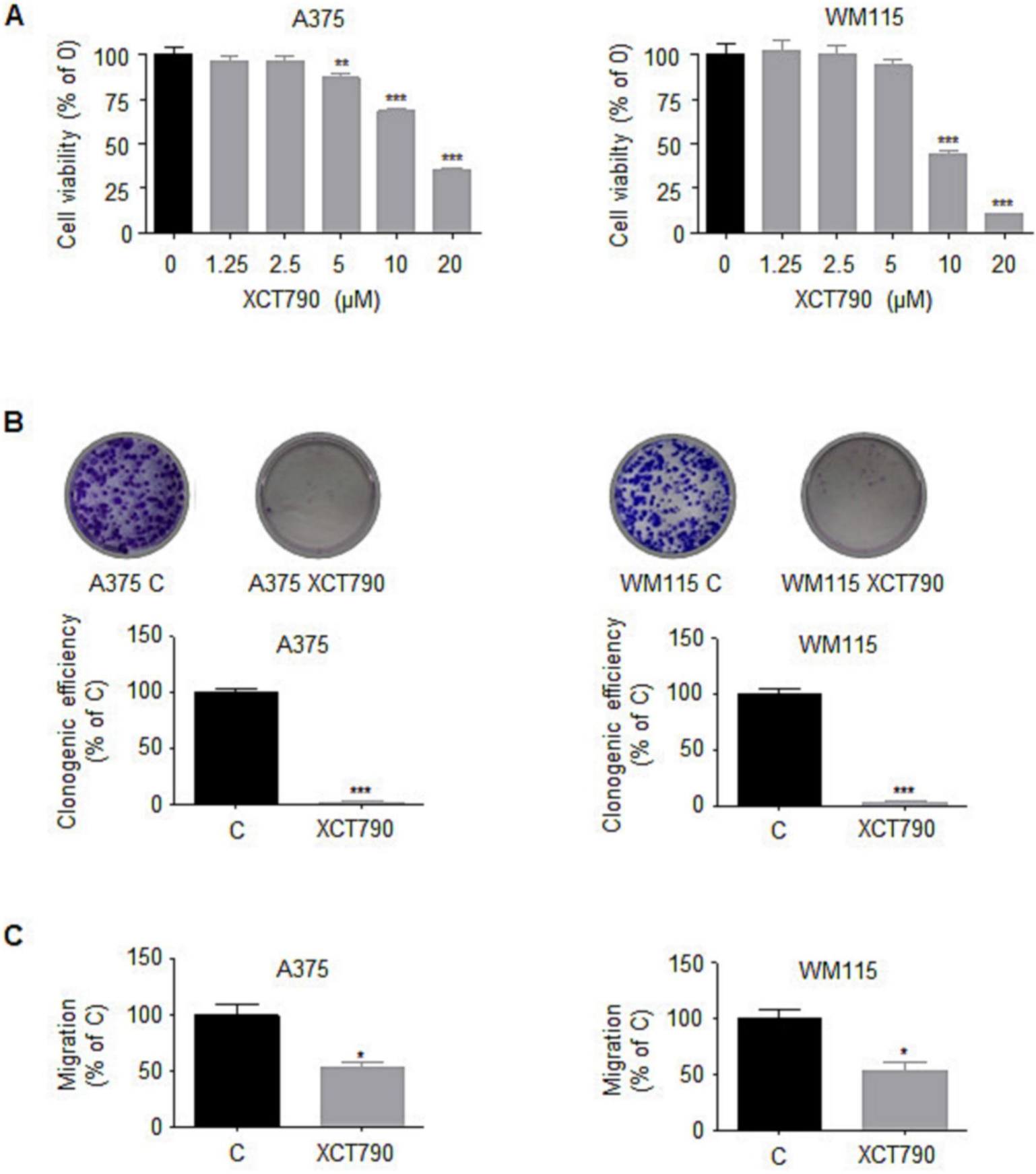
A
A375
Cell viability (% of 0)
100
75
50
25
0
**
***
***
0
1.25
2.5
5
10
20
XCT790 (μM)
WM115
Cell viability (% of 0)
***
***
XCT790 (μM)
B
A375 C
A375 XCT790
WM115 C
WM115 XCT790
Clonogenic efficiency (% of C)
150
100
50
0
A375
***
C
XCT790
WM115
***
C
Migration (% of C)
A375
*
WM115
*

Figure 5

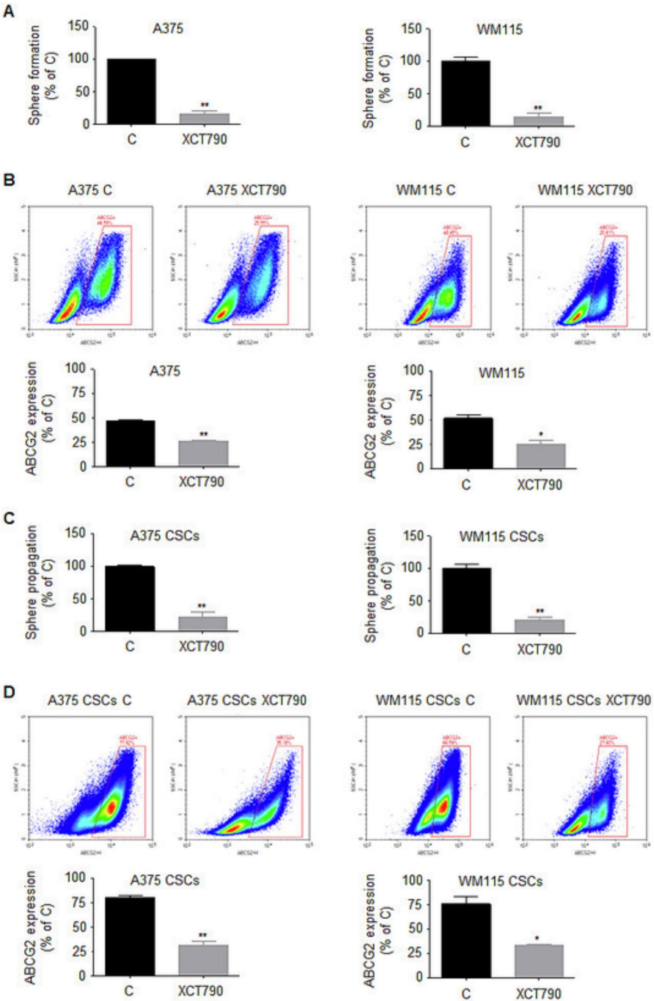
A
A375
Sphere formation (% of C)
150
100
50
0
**
C
XCT790
WM115
Sphere formation (% of C)
150
100
50
0
**
C
XCT790
B
A375 C
A375 XCT790
WM115 C
WM115 XCT790
A375
ABCG2 expression (% of C)
100
75
50
25
0
**
C
XCT790
WM115
ABCG2 expression (% of C)
100
75
50
25
0
*
C
XCT790
C
A375 CSCs
Sphere propagation (% of C)
150
100
50
0
**
C
XCT790
WM115 CSCs
Sphere propagation (% of C)
150
100
50
0
**
C
XCT790
D
A375 CSCs C
A375 CSCs XCT790
WM115 CSCs C
WM115 CSCs XCT790
A375 CSCs
ABCG2 expression (% of C)
100
75
50
25
0
**
C
XCT790
WM115 CSCs
ABCG2 expression (% of C)
100
75
50
25
0
*
C
XCT790

Figure 6

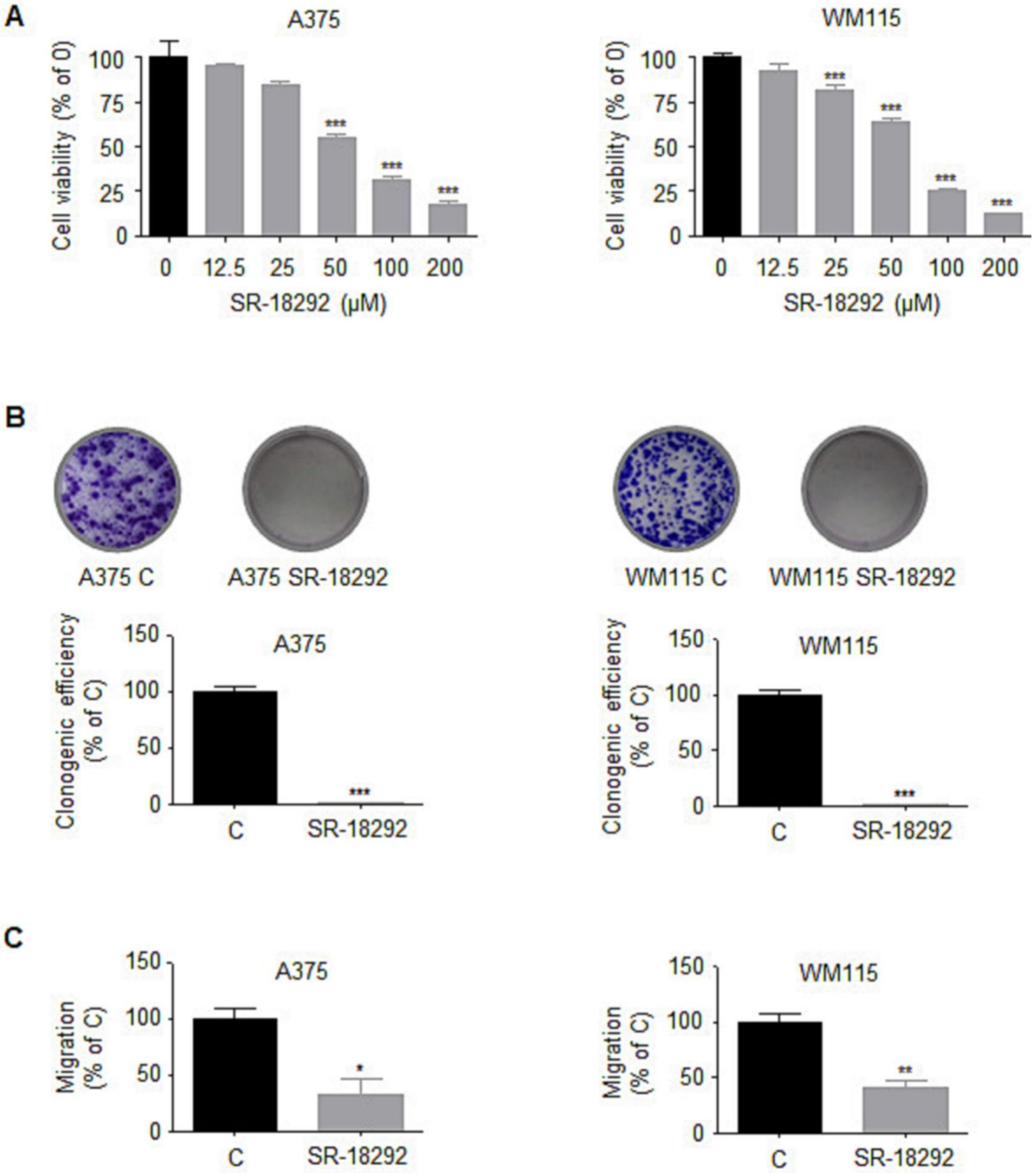
A
A375
Cell viability (% of 0)
100
75
50
25
0
***
***
***
0
12.5
25
50
100
200
SR-18292 (μM)
WM115
Cell viability (% of 0)
100
75
50
25
0
***
***
***
0
12.5
25
50
100
200
SR-18292 (μM)
B
A375 C
A375 SR-18292
WM115 C
WM115 SR-18292
Clonogenic efficiency (% of C)
A375
150
100
50
0
***
C
SR-18292
Clonogenic efficiency (% of C)
WM115
150
100
50
0
***
C
SR-18292
C
Migration (% of C)
A375
150
100
50
0
*
C
SR-18292
Migration (% of C)
WM115
150
100
50
0
**
C
SR-18292

Figure 7

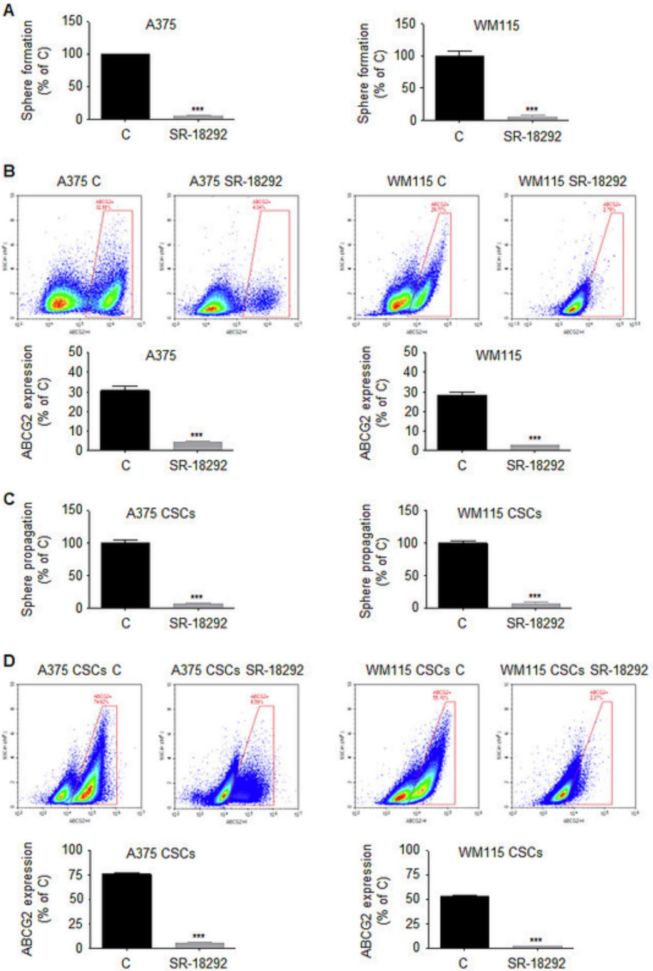
A
A375
Sphere formation (% of C)
150
100
50
0
***
C
SR-18292
WM115
Sphere formation (% of C)
B
A375 C
A375 SR-18292
WM115 C
WM115 SR-18292
ABCG2 expression (% of C)
40
30
20
10
C
SR-18292
C
A375 CSCs
Sphere propagation (% of C)
WM115 CSCs
D
A375 CSCs C
A375 CSCs SR-18292
WM115 CSCs C
WM115 CSCs SR-18292
75
25

Figure 8